Electronic Supplementary Material (ESI) for Nanoscale.

SUPPORTING INFORMATION

Distance dependent photoacoustics revealed through DNA nanostructures

Contents:

S1. DNA nanostructures nomenclature and design

Three series of nanostructures were prepared:

1. *Series **DQ***, with the structures carrying both dye and quencher. The DNA structures in this series are referred to as **Nnts-DQ**, where N indicates the number of nucleotides (nts) separating the dye and the quencher and **DQ** indicates that the structure contains both dye and quencher. Dye= IRDye 800CW or Cy5.5; Quencher= IRDye QC-1; N=0, 8, 11, 15, 21 and 31.
2. *Series **D***, with the structures carrying only the dye. The DNA structures in this series are referred to as **Nnts-D**. **D** indicates that the structure contains only dye. Dye= IR800CW or Cy5.5; N=0, 8, 11, 15, 21 and 31.
3. *Series **Q**,* with the structures carrying only the quencher. The DNA structures in this series are referred to as **Nnts-Q**. **Q** indicates that the structure contains only the IRDye QC-1 quencher. N=0, 8, 11, 15, 21 and 31.

The layout of the DNA nanostructures is shown in Figure S2. The sequences of all the composing oligonucleotides are illustrated in Table S1.

All our constructs were rationally designed to be composed by sequences that always contain the base “A” at the terminal end where either D or Q were attached. This was done to avoid that any quenching effect produced by the different nature of the base adjacent to the D and Q could affect the outcome of the results. The only exception was 0nts_1 oligonucleotide where the base next to the quencher had to be “T” since it needed to be hybridized with the “A” terminal base of 0nts_2.

We selected the base “A” next to the fluorophores and quencher based on the previous studies described by the supplier IDT on the effect that each of the four bases exert on the quenching on commonly used fluorophores where “A” presented low quenching.[1]

Importantly, our control structures having only D (series D) and only Q (series Q) were rationally designed to have the same sequences than the analogous DQ series to minimize the effect of any quenching arising from the otherwise different sequences.

To assess that there was no formation of quadruplexes or any other undesired folded structure we double checked the sequences composing our DNA nanostructures using NUPACK analysis tool.

S2. Förster Resonance Energy Transfer (FRET) calculations for fluorescent quenching

Intensity values used to calculate fluorescence quenching efficiency (FQE) were extracted at the peak wavelength of emission (794 nm and 704 nm for IRDye 800CW and Cy5.5 derivatives respectively). FQE values were plotted against the distance between dye and quencher (R), which was estimated by multiplying N (number of nucleotides separating dye and quencher) by 0.34 nm^2 (Figure 2 in the main text). These data were fitted using the equation described for calculating the FRET efficiency (E), namely $\mathbf{E= 1/(1+(R/R_0)^6)}$ (dotted line in Figure 2 in the main text). This nonlinear curve fit was achieved using Orthogonal Distance Regression (ODR) with OriginPro2016. These relationships show r^2 values of 0.987 (IRDye 800CW) and 0.997 (Cy5.5). R_0 is the distance at which 50% FRET efficiency is observed; R_0 was estimated to be 5.6±0.8 nm and 4.4±0.5 nm for IRDye 800CW/IRDye QC-1 and cy5.5/IRDye QC-1 pairs respectively. For IRDye 800CW/IRDye QC-1, R_0 was previously reported to be 6.5 nm according to calculations performed based on the optical properties (absorbance, emission and quantum yield) of free dyes and quenchers in methanol solutions.[3] The discrepancy between these two estimates of R_0 is minor and is likely due to a difference in the solvents (methanol vs phosphate buffered saline) and the chemical environment (the optically active molecules here are linked to DNA rather than as free species in solution).[4] It could also arise from differences between the estimated and actual distance between D and Q in each DNA nanostructure.[5] While more precise distance estimates than those used here could be achieved using molecular models[6] and/or molecular dynamic simulations[7], several unknown parameters for our studied D-Q pairs would need to be elucidated for these to be conducted reliably,[8] hence it was considered beyond the scope of the present study.

S3. Förster Resonance Energy Transfer (FRET) calculations for photoacoustic enhancement

Photoacoustic enhancement (PE) values were calculated as described in the main text. The values were plotted against distance as explained in Supporting Information Section S2. We assumed there is a linear relationship between the FRET efficiency measured by fluorescence and the PE and hence these data were fitted using the equation described for calculating the FRET efficiency (E) (dotted line in Figure 4(a) and (b) in the main text) in which a correction "enhancement" factor **"A"** is also obtained from the fitted data. Namely, PE depends on the inverse sixth power of R (the separation distance between dye and quencher), $\mathbf{PE= A*(1/(1+(R/R_0)^6)}$). This nonlinear curve fit was achieved using Orthogonal Distance Regression (ODR) with OriginPro2016. These relationships show r^2 values of 0.998 (IRDye 800CW) and 0.988 (Cy5.5). "A" values are estimated to be 96±6 (PE(%)) and 274±29 (PE(%)) for IRDye 800CW/IRDye QC-1 and cy5.5/IRDye QC-1 pairs respectively. $\mathbf{R_0}$ values are estimated to be 4.3±0.2 nm and 5.0±0.8 nm for IRDye 800CW/IRDye QC-1 and cy5.5/IRDye QC-1 pairs respectively. Note that although we have experimentally found that fluorescence quenching and PA follow the same dependence with R (proportional to $1/(1+(R/R_0)^6)$, the calculated R_0 values do not coincide. Further theoretical understanding of these processes would be needed to understand whether these R_0 values should in fact match, given that fluorescence quenching and PA enhancement occur through different physical mechanisms.

S4. Constructing a computational model for 0nts-DQ

The strong differences of the experimental absorption spectra of the 0nts-DQ systems in comparison with spectra from the N=8-31nts series, namely the blue shift of the main absorption peak and the formation of a shoulder in the longer wavelengths, are thought to be caused by a direct interaction between the dye and the quencher molecule, facilitated by their close proximity for N=0 nts. In order to test this hypothesis, we construct a simple computational model of an interacting dye-quencher system.

We argue that a likely candidate for a direct interaction between dye and quencher responsible for spectral changes is a simple dipole coupling of the excited state on the dye with that on the quencher. Two coupled, localized excited states that interact via their dipoles have the tendency to form two delocalized excitons, one in a dipole-opposed configuration with lower oscillator strength and energy, and one in a dipole-aligned configuration with enhanced oscillator strength and increased energy. This simple picture is closely followed by the experimental absorption spectra for 0nts-DQ.

Having formed the hypothesis that dipole-coupled excited states are the likely source of spectral changes in the 0nts-DQ, we construct a simple computational model of a dye-quencher system where the dipole-dipole coupling is maximized. This is achieved by stacking the dye and quencher on top of each other such that their excited state transition dipole moments are aligned, and optimizing the structure of the dimer using DFT. We note that this model conformation is likely stabilized by attractive π-stacking between the two molecules (Figure S10).

The simple computational model considered here does not include the effects of temperature or explicit solvent interactions and can therefore not be expected to reproduce experimental line shapes. Furthermore, all calculations are performed on the reduced model

structures of the dye and the quencher and the attachment to the DNA is not included in the computational study. Nevertheless, the fact that the simulated spectra of the simple model system provide a good qualitative match to the experimental results for 0nts-DQ can be seen as strong evidence that a stacking of the dye and the quencher is responsible for the observed changes in the absorption spectra. Table S7 details the energies and oscillator strengths of the two coupled excitons that make up the strong absorption peak at approximately 600 nm in simulated absorption spectra in the combined mode system. It also shows a breakdown of the excitons into contributions from the bright S1 state of the dye and S2 state of the quencher. The data shows that the combined dye-quencher systems indeed form excitons in a dipole-opposed configuration with lower oscillator strength and energy, and dipole-aligned configurations with increased energy and oscillator strength.

SUPPORTING FIGURES

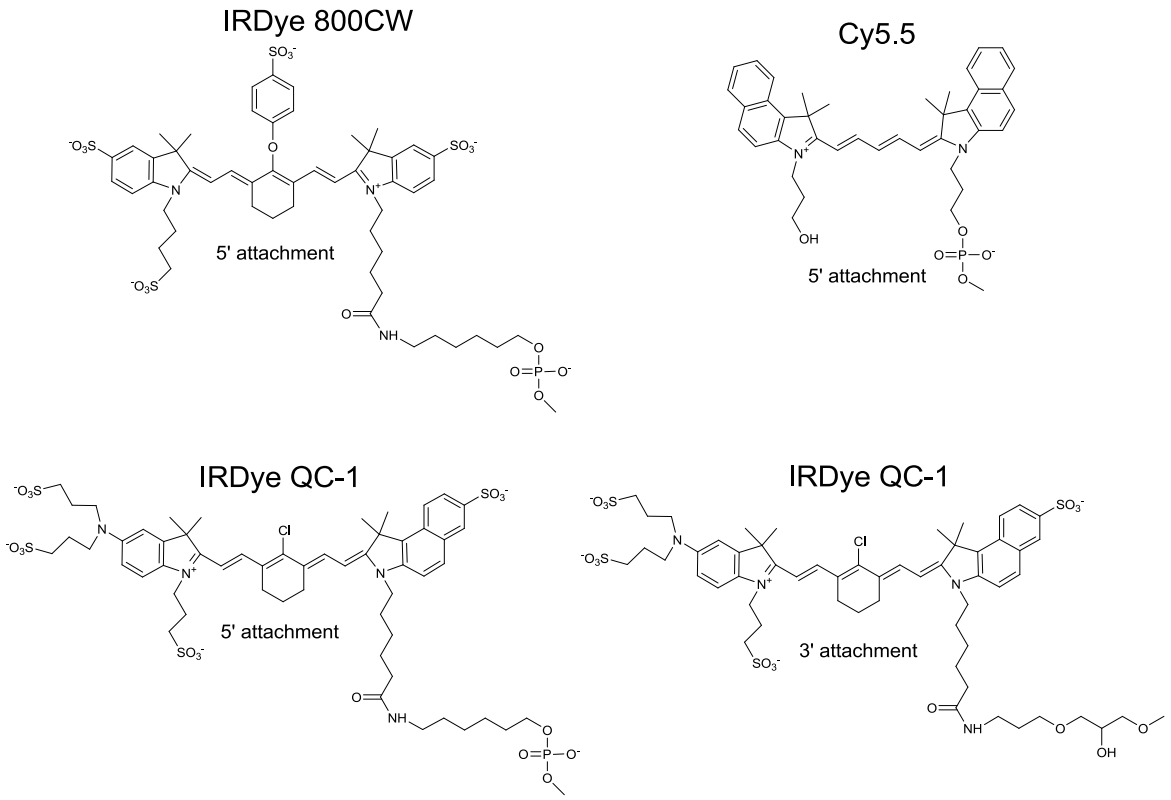

Figure S1. Chemical structure of IRDye 800CW, Cy5.5 and IRDye QC-1 (including its attachment into DNA).

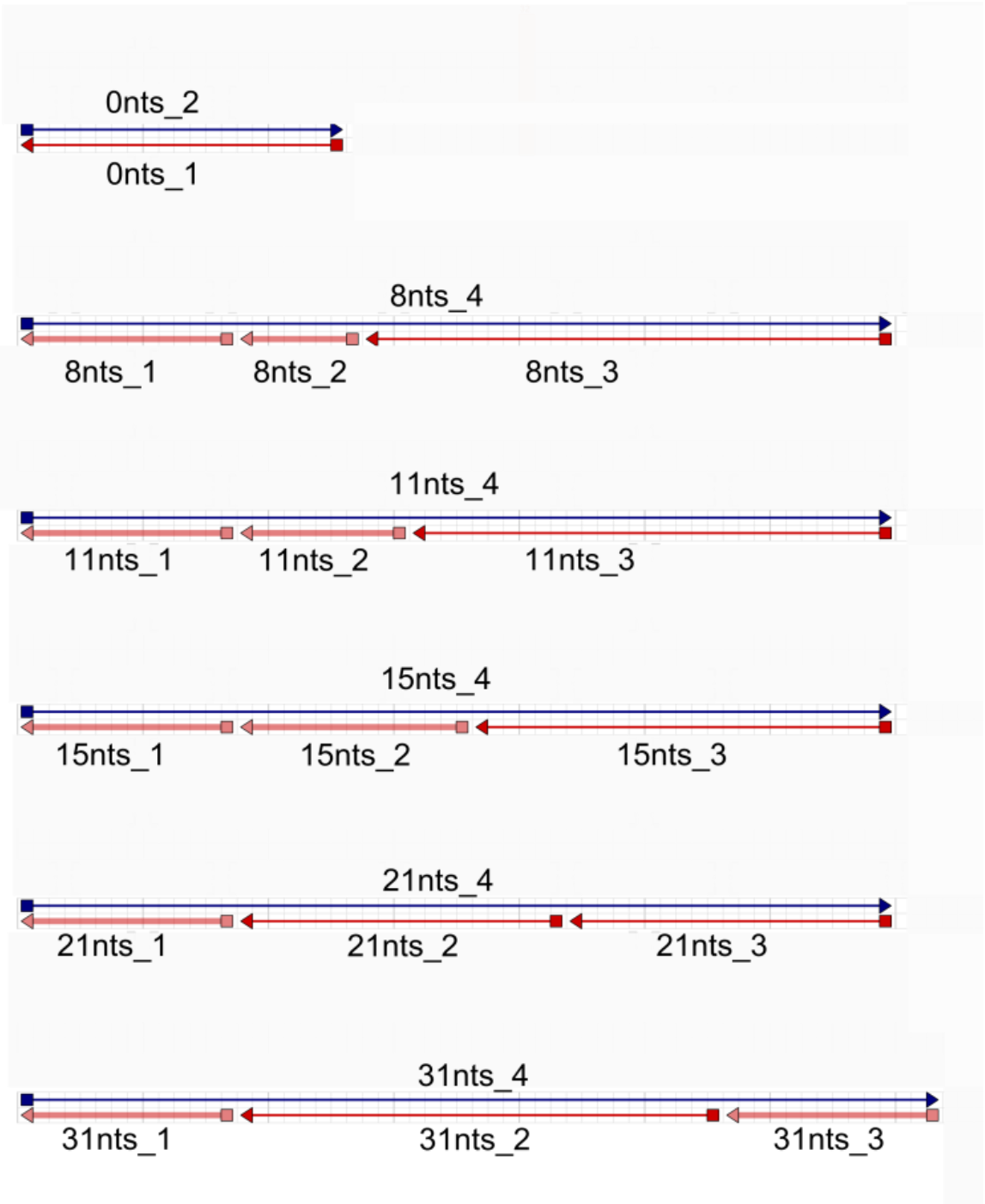

Figure S2. Layout showing the assigned strands composing the DNA nanostructures.

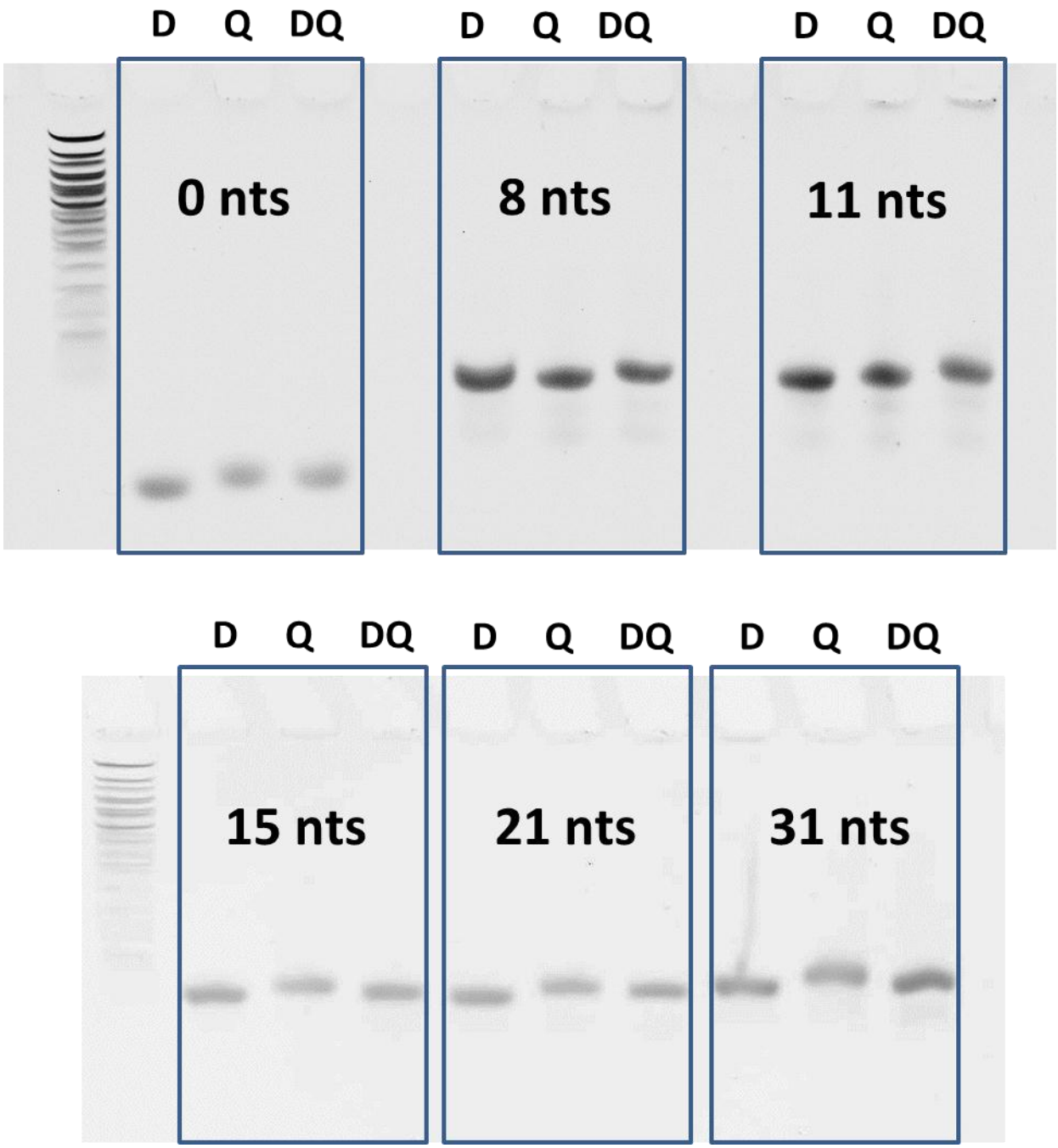

Figure S3. PAGE gel of the Nnts D, Nnts Q and Nnts DQ nanostructures (N= 0, 8 and 11 nts in the top panel and N= 15, 21 and 31 nts in the bottom panel). Each nanostructure resolves into a single band that is evidence for the correct folding. 0-nts derivatives ran faster due to the small size of the nanostructure. DNA ladder is included in the left lane of each gel.

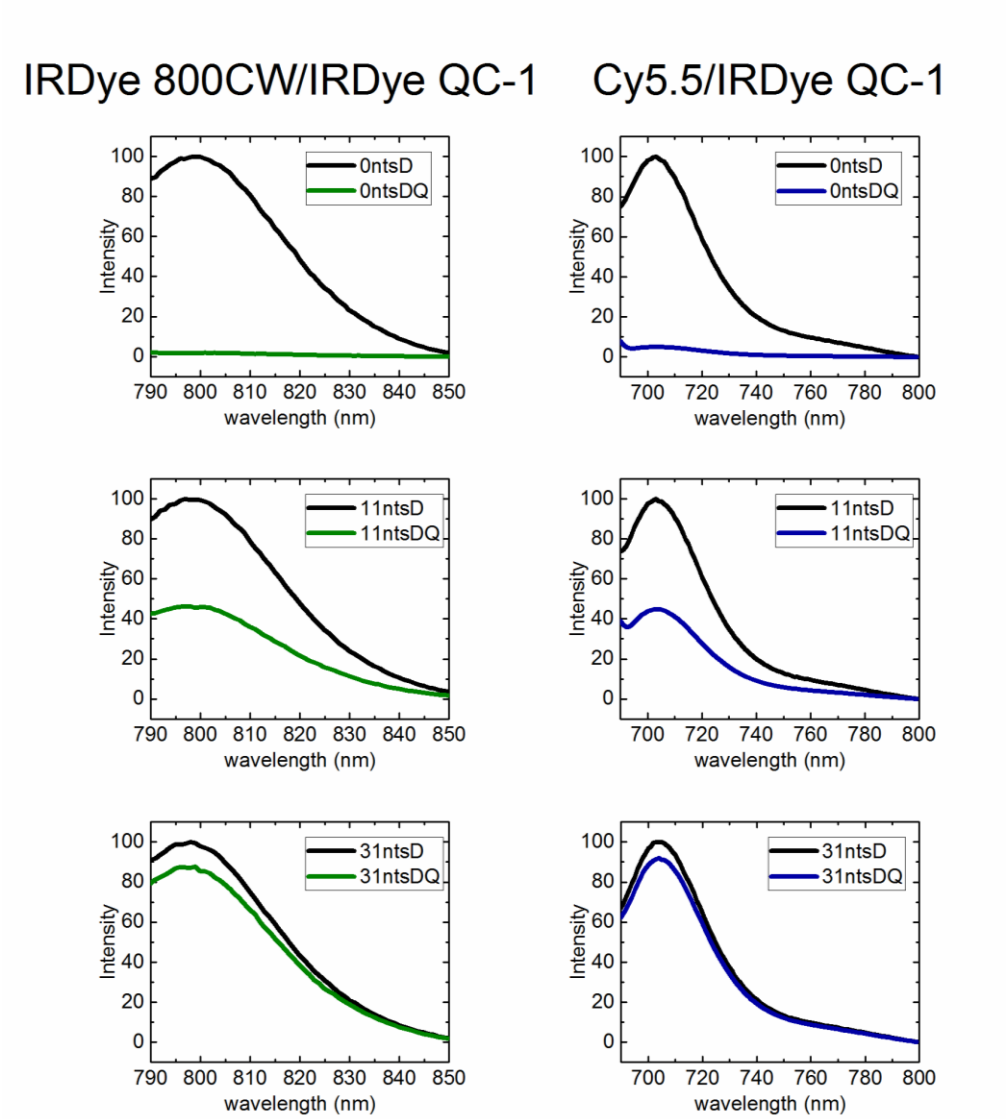

Figure S4. Representative example of the emission spectra of the Nnts_D and Nnts-DQ structures in IR800CW and cy5.5 derivatives with N=0nts, 11nts and 31nts of series. Intensities are normalized to the Nnts_D derivatives.

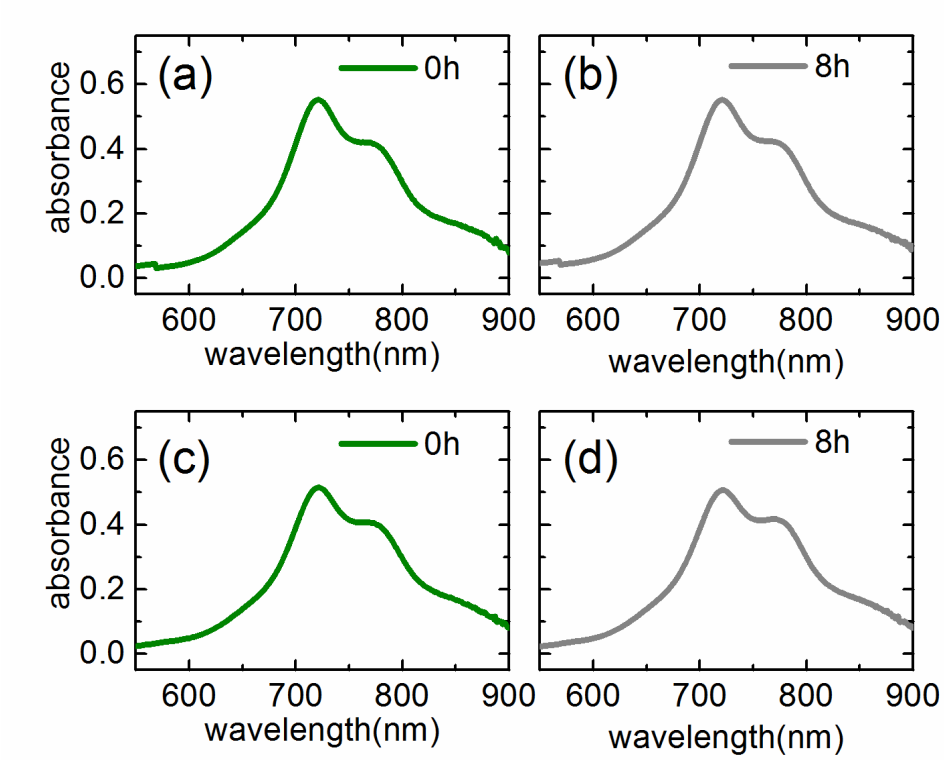

Figure S5. Absorbance spectra of the 0nts_DQ DNA structure (IRDye 800cw/IRDye QC-1 derivative) after incubation in PBS at 34°C (a) at time zero and (b) after 8 hours. After incubation in DMEM media (no phenol red) with 10% FCS at 37°C (c) at time zero and (d) after 8 hours.

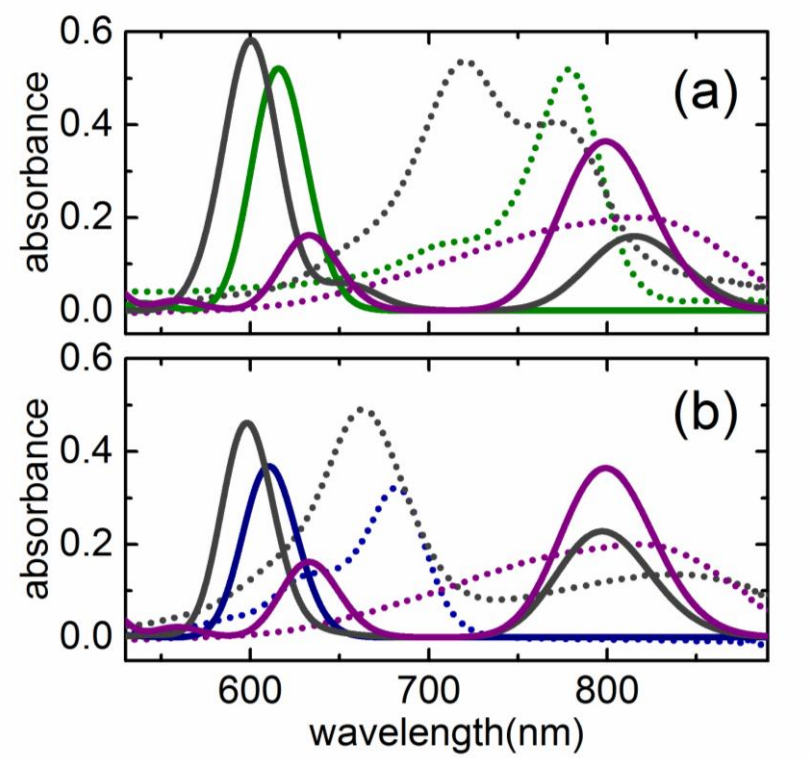

Figure S6. Comparison of theoretical and experimental absorbance obtained from 0nts DNA nanostructures as predicted by TDDFT calculations. (a) Spectra for IR800CW derivatives. (b) Spectra for Cy5.5 derivatives. Theoretical spectra are shown as solid lines and the corresponding experimental data as dotted lines. 0nts-DQ in dark grey, 0nts-Q in purple and 0nts-D in green (IR800CW) and blue (Cy5.5) respectively.

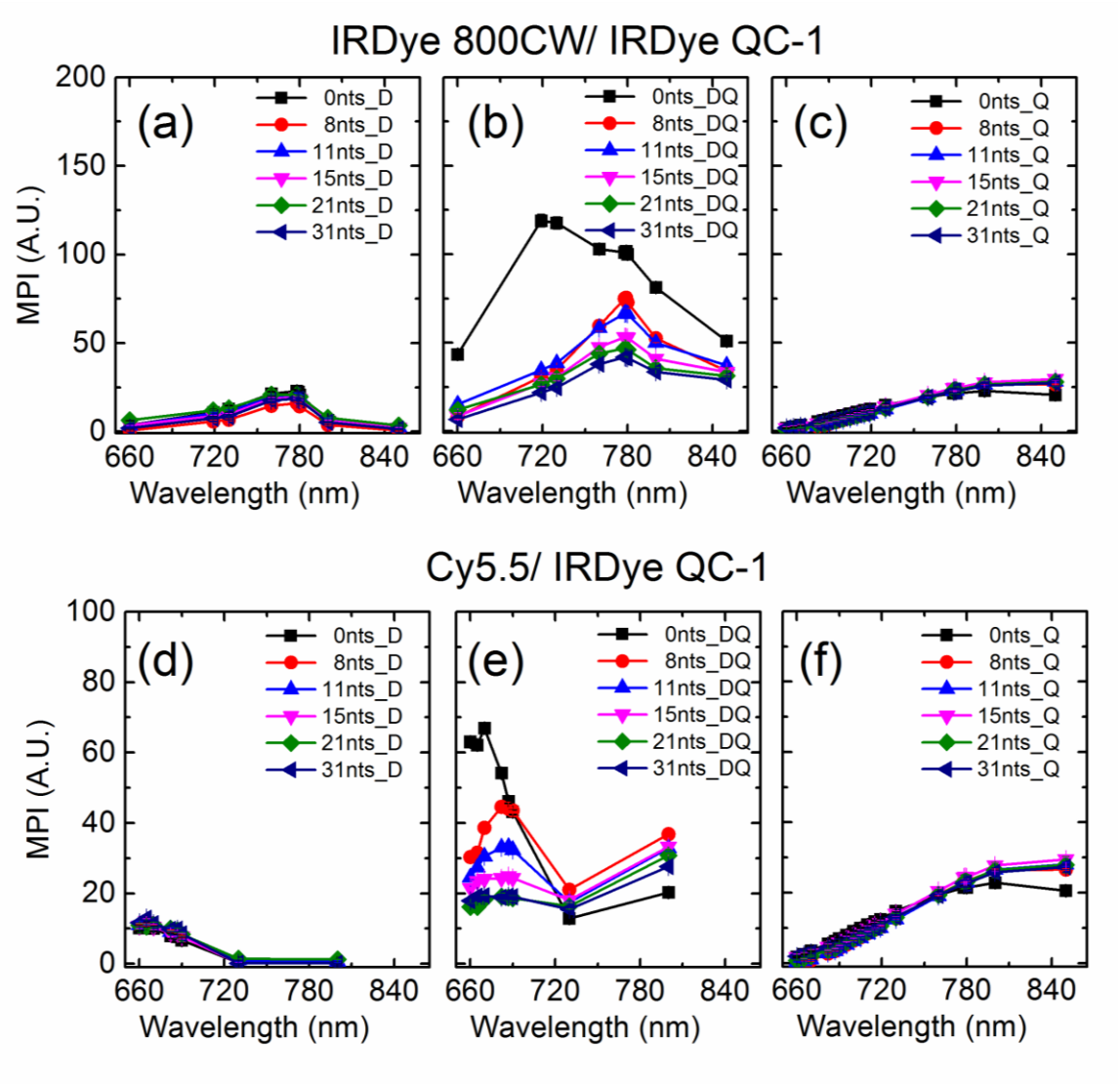

Figure S7. Photoacoustic spectra for the different DNA nanostructures. (a) Nnts-D derivatives containing the IRDye 800CW. (b) Nnts-DQ derivatives containing the IRDye 800CW and the IRDye QC-1. (c) and (f) Nnts-Q derivatives containing the IRDye QC-1. (d) Nnts-D derivatives having the Cy5.5. (e) Nnts-DQ derivatives containing the Cy5.5 and the IRDye QC-1.

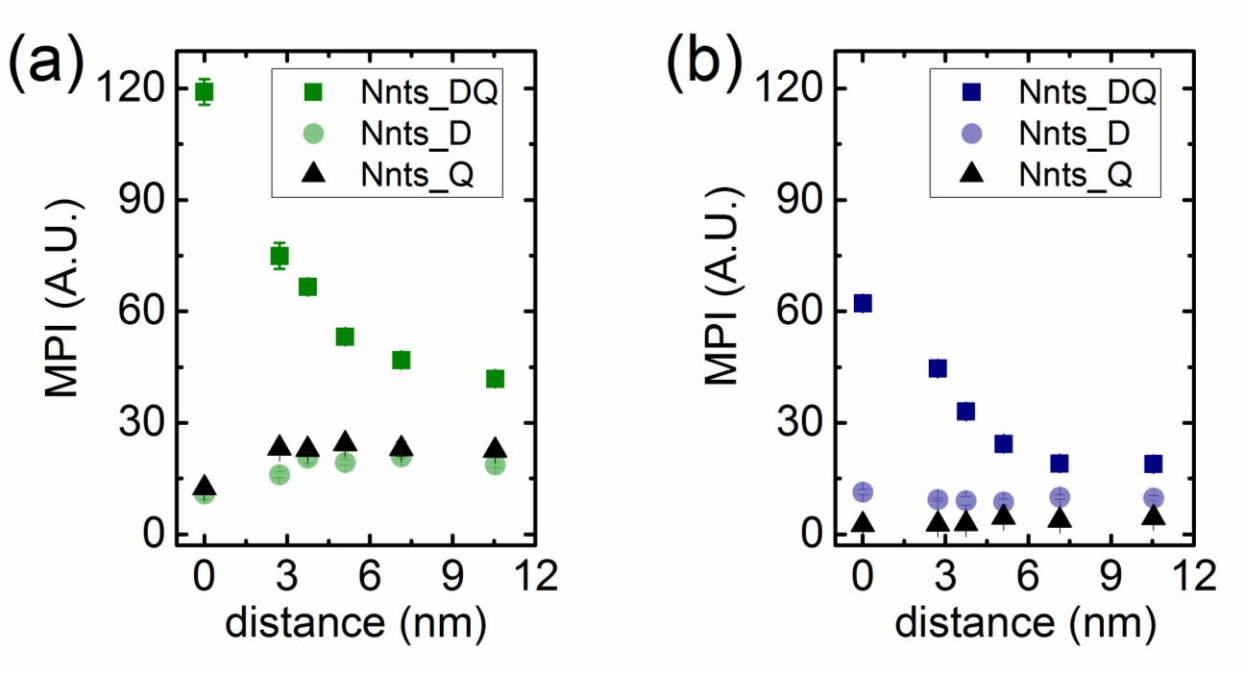

Figure S8. Photoacoustic response derived from the mean pixel intensity (MPI) values extracted from the region of interest (ROI) for the different DNA nanostructures at their respective peak absorption wavelengths. (a) IR800CW derivatives (green) and (b) Cy5.5 derivatives (blue). Note that the values shown by Nnts-Q differ depending on the nanostructure under study (IR800CW or Cy5.5 derivatives) due to the different wavelengths at which the MPI values were calculated (see Table S6).

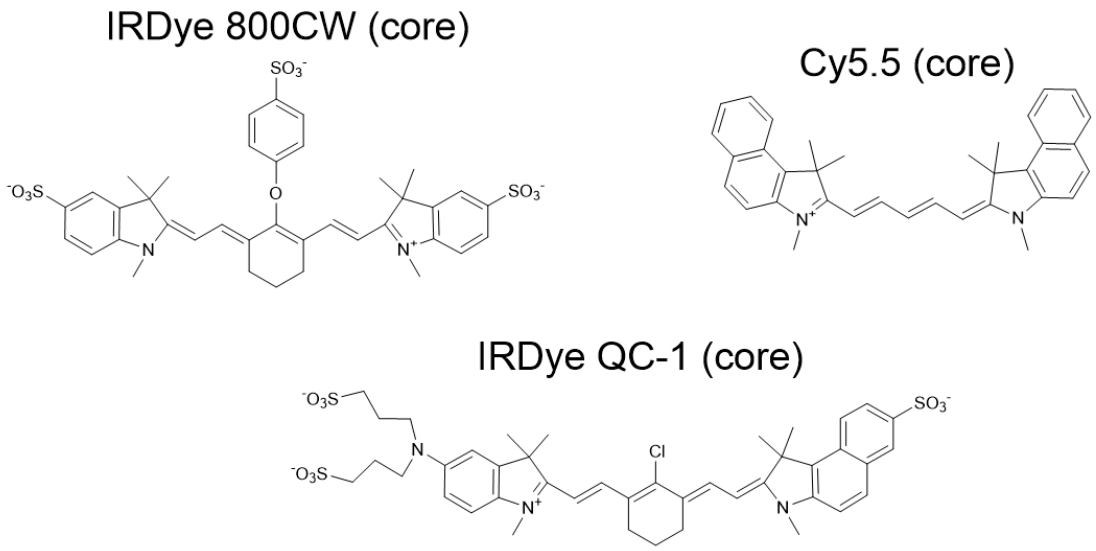

Figure S9. Reduced chemical structures of IRDye 800CW, IRDye QC-1 and Cy5.5 used for TDDFT calculations.

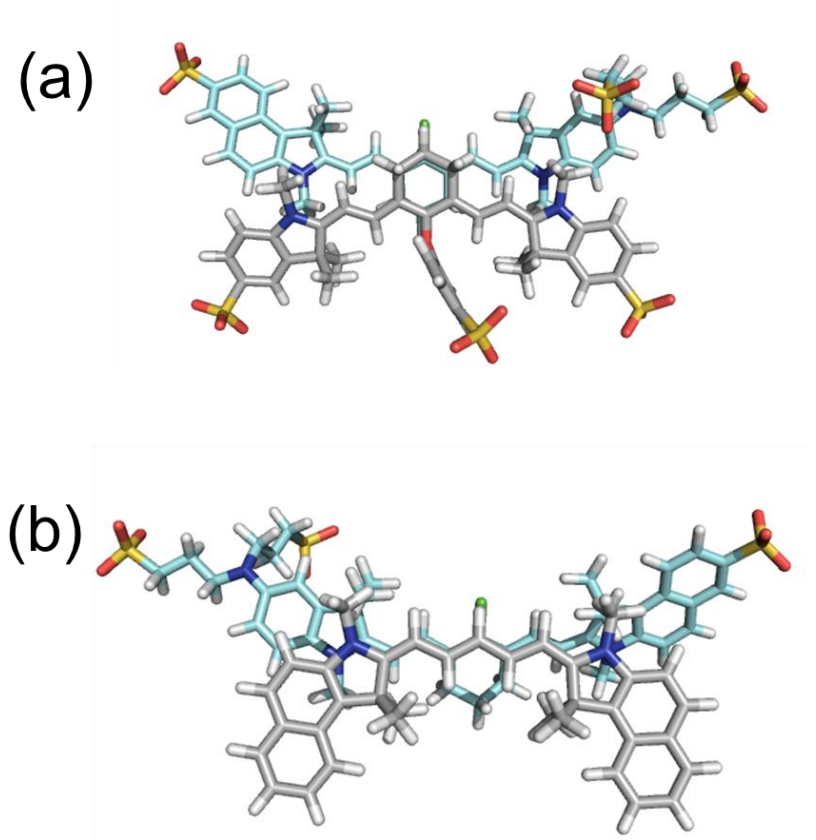

Figure S10. Optimized structures for the stacked dye-quencher models of (a) IR800Dye CW/ IRDye QC-1 and (b) Cy5.5/ IRDye QC-1 used in the TDDFT calculations. The carbon atoms belonging to the quencher are colored in light blue, while the carbon atoms of the dyes are shown in grey. Note the alignment of the backbones of the dye and the quencher in both model systems are chosen to maximize the dipole coupling of the dominant excitations in the dye and the quencher.

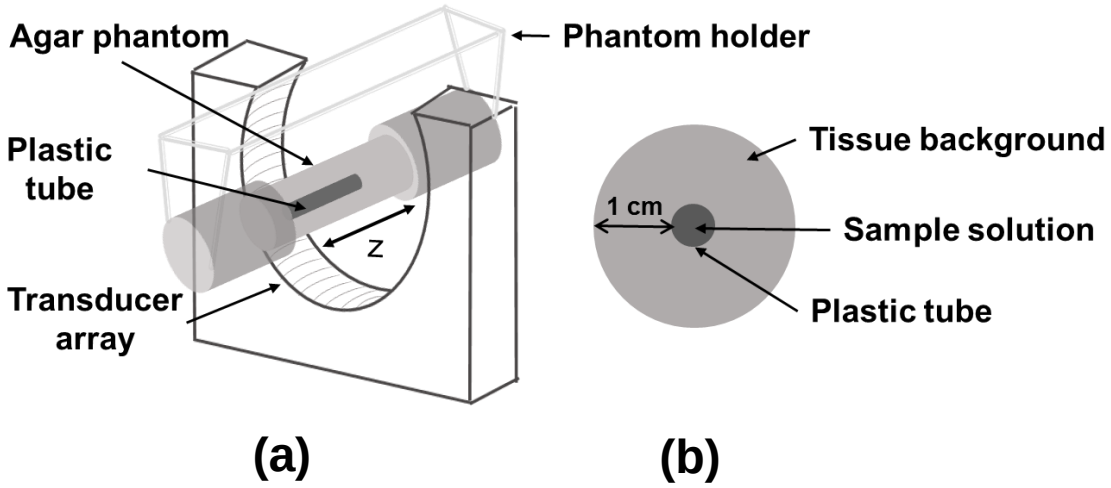

Figure S11. Illustration of the photoacoustic tomography geometry for imaging of tissue mimicking agar phantoms. (a) Schematic of sample positioning within the imaging chamber. (b) Cross-sectional view of the sample positioned inside the tissue mimicking phantom.

SUPPORTING TABLES

Table S1. Oligonucleotides sequences used for synthesizing the nanostructures. The dye and quencher are attached at either 5' or 3' position (terminal position in the oligonucleotide). The precise position for the attachment of the dye and quencher is marked in red and blue respectively.

0nts	
0nts_1	CCATCCGATCATAGACAGAA**T**
0nts_2	**A**TTCTGTCTATGATCGGATGG
8nts	
8nts_1	**A**CACTTTCACCTCT
8nts_2	**A**GCTCGGC
8nts_3	GTACGAGTATTGTGTGCTTAATTTCTGTCTAATG
8nts_4	AGAGGTGAAAGTGTGCCGAGCTCATTAGACAGAAATTAAGCACACAATACTCGTAC
11nts	
11nts_1	**A**CACTTTCACCTCT
11nts_2	**A**GATCGGATGG
11nts_3	GTACGAGTATTGTGTGCTTAATTTCTGTCTA
11nts_4	AGAGGTGAAAGTGTCCATCCGATCTTAGACAGAAATTAAGCACACAATACTCGTAC
15nts	
15nts_1	**A**CACTTTCACCTCT
15nts_2	**A**CTATGATCGGATGG
15nts_3	GTACGAGTATTGTGTGCTTAATTTCTG
15nts_4	AGAGGTGAAAGTGTCCATCCGATCATAGTCAGAAATTAAGCACACAATACTCGTAC
21nts	
21nts_1	**A**CACTTTCACCTCT
21nts_2	**A**TTCTGTCTATGATCGGATGG
21nts_3	GTACGAGTATTGTGTGCTTAA
21nts_4	AGAGGTGAAAGTGTCCATCCGATCATAGACAGAATTTAAGCACACAATACTCGTAC
31nts	
31nts_1	**A**CACTTTCACCTCT
31nts_2	**A**TGTGCTTAATTTCTGTCTATGATCGGATGG
31nts_3	CTTTATGGATACGG
31nts_4	AGAGGTGAAAGTGTCCATCCGATCATAGACAGAAATTAAGCACATCCGTATCCATAAAG

Table S2. Wavelengths used for fluorescence emission measurements

	IRDye 800CW N= 8 to 31nts	***Cy5.5 N= 8 to 31nts***	***IRDye 800CW N= 0 nts***	***Cy5.5 N= 0 nts***
Wavelengths	778nm	684nm	719nm	664nm

Table S3. Excitation wavelengths used for PAT measurements

Series	***Wavelengths (nm)***
Nnts-D and Nnts-DQ: IR800CW derivatives	660, 719, 730, 760, 778, 779, 780, 800, 850
Nnts-D and Nnts-DQ: Cy5.5 derivatives	660, 665, 670, 682, 687, 690, 730, 800
Nnts-Q: IR800CW and Cy5.5 derivatives	660, 665, 670, 682, 687, 690, 695, 700, 705, 710, 715, 719, 730, 760, 778, 779, 780, 800, 850

Table S4. MPI values obtained by PAT for the IRDye 800CW-IRQC$_1$ derivatives extracted at the wavelengths shown in table S6

	Nnts-D		**Nnts-DQ**		**Nnts-Q**	
N	*Average*	*Std*	*Average*	*Std*	*Average*	*Std*
0	10874	1503	119054	3447	12468	122
8	16046	806	74953	3488	23161	212
11	20524	1481	66585	1220	22848	370
15	19361	756	53165	1945	24355	805
21	20876	296	46904	477	23041	1959
31	18698	668	41882	1434	22595	932

Table S5. MPI values obtained by PAT for the Cy5.5-IRQC$_1$ derivatives extracted at the wavelengths shown in table S6

	Nnts-D		***Nnts-DQ***		***Nnts-Q***	
N	*Average*	*Std*	*Average*	*Std*	*Average*	*Std*
0	11391	720	62147	486	2568	53
8	9391	360	44596	378	2728	233
11	9070	1143	33065	794	2854	306
15	8718	785	24337	871	4563	894
21	10023	645	19102	985	3780	335
31	9769	661	18888	598	4433	1230

Table S6. Wavelengths used for the calculation of the MPI values obtained from PAT measurements

	IRDye 800CW N= 8 to 31nts	***Cy5.5 N= 8 to 31nts***	***IRDye 800CW N= 0nts***	***Cy5.5 N= 0nts***
Wavelengths	778nm	682nm	719nm	665nm

Table S7. Characteristics of the main absorption peaks in the simulated absorption spectra.

Dye	Wavelength (nm)	Oscillator Strength	Excitation Character
IRDye 800CW	654	0.21	50% S2 quencher, 26% S1 dye
	601	2.05	49% S1 dye, 18% S2 quencher
Cy5.5	640	0.04	40% S2 quencher, 23% S1 dye
	598	1.68	30% S1 dye, 13% S2 quencher

REFERENCES

1. http://biophysics.idtdna.com/pdf/Fluorescence_quenching_by_proximal_G_bases.pdf *(date accessed 09/2017)*.
2. C. E. Castro, F. Kilchherr, D.-N. Kim, E. L. Shiao, T. Wauer, P. Wortmann, M. Bathe and H. Dietz, *Nat. Meth.*, 2011, **8**, 221-229.
3. X. Peng, H. Chen, D. R. Draney, W. Volcheck, A. Schutz-Geschwender and D. M. Olive, *Anal. Biochem.*, 2009, **388**, 220-228.
4. A. Periasamy and R. Day, *Molecular imaging: FRET microscopy and spectroscopy*, Elsevier, 2011.
5. S. Sindbert, S. Kalinin, H. Nguyen, A. Kienzler, L. Clima, W. Bannwarth, B. Appel, S. Müller and C. A. Seidel, *J. Am. Chem. Soc.*, 2011, **133**, 2463-2480.
6. R. M. Clegg, A. I. H. Murchie, A. Zechel and D. M. J. Lilley, *Proc. Natl. Acad. Sci. U. S. A.*, 1993, **90**, 2994-2998.
7. A. K. Woźniak, G. F. Schröder, H. Grubmüller, C. A. M. Seidel and F. Oesterhelt, *Proc. Natl. Acad. Sci. U. S. A.*, 2008, **105**, 18337–18342.
8. I. H. Stein, V. Schüller, P. Böhm, P. Tinnefeld and T. Liedl, *ChemPhysChem*, 2011, **12**, 689-695.